Detection and Isolation of Small Faults in Lithium-Ion Batteries via the Asymptotic Local Approach*

Luis D. Couto[1,2], Jorn M. Reniers[1], David A. Howey[1,3] and Michel Kinnaert[2]

Abstract— **This contribution presents a diagnosis scheme for batteries to detect and isolate internal faults in the form of small parameter changes. This scheme is based on an electrochemical reduced-order model of the battery, which allows the inclusion of physically meaningful faults that might affect the battery performance. The sensitivity properties of the model are analyzed. The model is then used to compute residuals based on an unscented Kalman filter. Primary residuals and a limiting covariance matrix are obtained thanks to the local approach, allowing for fault detection and isolation by χ^2 statistical tests. Results show that faults resulting in limited 0.15% capacity and 0.004% power fade can be effectively detected by the local approach. The algorithm is also able to correctly isolate faults related with sensitive parameters, whereas parameters with low sensitivity or linearly correlated are more difficult to precise.**

I. INTRODUCTION

Lithium-ion (Li-ion) batteries are all around us, from mobile phones to electric vehicles. This ubiquity comes from the fact that these energy storage devices have a high energy and power density, compared with other types of batteries [1]. However, this improved performance comes at the cost of safety issues, such as possible short circuit or thermal runaway [2], if Li-ion batteries are mistreated. A common way to prevent possible safety hazards in Li-ion batteries is to oversize them, which results in more bulky and expensive batteries whose operation is overly conservative [1]. An alternative way to guarantee safe operation without incurring unnecessary cost is to monitor battery condition through model-based approaches. Among other tasks, such a monitoring system is in charge of performing battery diagnostics, i.e. detection and isolation of possible faults affecting battery operation. In this context, special emphasis is placed on early warnings in order to prevent failure and predict maintenance.

Efforts in fault diagnostics for Li-ion batteries have grown in recent years [2]. They fall into two main categories depending on the diagnostic method used, namely data-driven and model-based methods [2]. Data-driven methods provide high-order nonlinear approximations that are versatile to accommodate the estimated faults in relation to the measured data, but they suffer from requiring large and rich fault datasets for model training and they are disconnected from physical principles. These pitfalls are overcome by model-based methods. This second category of methods aims at detecting and isolating changes in greybox model parameters, which are linked to the state-of-health of the battery. Within this category, a first and the most popular approach is to estimate both parameters & states using parameter estimators in conjunction with state observers, for example by augmented states (to include parameters) or adaptive observers. Parameter estimation alone has been performed by using optimization-based techniques, such as the Levenberg–Marquardt method [3] and the Gauss–Newton method [4], as well as parameter identification algorithms such as recursive least-squares [5], [6] and instrumental variables [7]. Augmented state observers include Kalman filters (KF) [8], [5], [9], particle filters [10] and nonlinear geometric observers [11]. Adaptive observers combine a state observer for state estimation with another estimator for determining the parameters [12], [13], [14], [15]. For all these observer-based methods, identifiability issues may arise from the state/parameter interplay, and an additional decision system is needed to analyze the evolution of the model parameters as well as evaluate their significance with respect to estimation error.

In contrast with state/parameter estimation, a second approach within model-based methods is residual-based, which involves state observers or parity relations. Some approaches deal with state-of-health indication only, where a bank of observers has been used to generate residuals for the fault detection and isolation (FDI) of battery faults like resistance increase [16] and over(dis)charge [17]. Others also consider sensor faults and use Kalman filters [18], [19] and sliding-mode observers [20]. Finally, sensor and/or actuator faults together with battery aging has been addressed via robust observers [21], Kalman filters [22] and structural analysis [23]. However, methods relying exclusively on the innovation sequence are not appropriate to detect parametric changes, because in that case the innovation is not a sufficient statistic[1]. Moreover, methods based on nonlinear parity equations also require the development of an appropriate decision system which might not be easy because the residual pattern will typically depend on the operating conditions.

[1]L.D. Couto (luis.coutomendonca@eng.ox.ac.uk), J.M. Reniers (jorn.reniers@eng.ox.ac.uk) and D.A. Howey (david.howey@eng.ox.ac.uk) are with the Department of Engineering Science, University of Oxford, Oxford OX1 3PJ, UK.

[2]L.D. Couto and M. Kinnaert (michel.kinnaert@ulb.ac.be) are with with the School of Engineering of the Université Libre de Bruxelles, B-1050 Brussels, Belgium.

[3]D.A. Howey is also with the Faraday Institution, Harwell Campus, Didcot, OX11 0RA, UK.

[1]We say that a statistic S is *sufficient* if the information about the model parameter θ contained in the sample $\mathcal{Y}$ is concentrated in the statistic S. See [24] for more details.

In this paper, we depart from the previous works by exploiting a specific type of residual which provides a sufficient statistic for parametric change detection and which lends itself to a sound statistical approach for detection and isolation of small faults via the so-called local approach [25]. We investigate how this approach can be applied for early warning of degradation in lithium-ion batteries, which may help to sort batteries in terms of performance at the beginning of life. A reduced-order electrochemical model of the battery is used to obtain a physical interpretation of the parametric changes. We also analyze the correlation between the obtained results for fault detection and isolation and a sensitivity study of the measurements to parametric changes, enabling more insight into the results.

II. ELECTROCHEMICAL MODELING

Given its physical basis and therefore the possibility to account for realistic faults, an electrochemical model of the battery cell is considered. In this section, we first introduce the reduced-order electrochemical model used to describe the healthy operation of a battery cell, followed by the possible fault modes that we consider in this work.

A. Healthy operation

An equivalent-hydraulic model (EHM) [14] is used to represent the electrochemical behaviour of a battery system. In a general sense, this model is mathematically described by the following discrete-time nonlinear dynamical system:

$$x(k+1) = f(\theta, x(k), u(k)), \tag{1}$$
$$y(k) = h(\theta, x(k), u(k)), \tag{2}$$

where the state vector consists of the state-of-charge and normalized surface concentration $x = [\text{SOC} \quad \bar{c}_{ss}]^\top$, the input is the applied current $u = I$ and the output is the terminal voltage $y = V$. The parameter vector is $\theta = [\varepsilon_s^- \ R_f \ g_s \ n_{Li}]^\top$, which comprises possibly aging-related parameters. These parameters are the active material volume fraction ε_s, the film resistance R_f, the inverse of the diffusion time constant g_s and the moles of lithium n_{Li}.

Generally, each electrode should be described by an EHM, however here we introduce two common assumptions that reduce the model dynamics to a single EHM. First, the positive electrode dynamics are faster than the negative electrode dynamics, which means that the SOC^+ and $\bar{c}_{ss}^+$ dynamics are the same as in $\text{SOC}^+ = \bar{c}_{ss}^+$. Secondly, the total moles of lithium in the battery is the sum of the amount of lithium in positive and negative electrodes, i.e.

$$\frac{n_{Li}}{A} = c_{s,\max}^+ L^+ \varepsilon_s^+ \text{SOC}^+ + c_{s,\max}^- L^- \varepsilon_s^- \text{SOC}^-, \tag{3}$$

which can be solved for SOC^+ and written as $\text{SOC}^+ = \theta_1 \rho \text{SOC}^- + \theta_4 \sigma$ with $\rho = -c_{s,\max}^- L^- / (c_{s,\max}^+ L^+ \varepsilon_s^+)$ and $\sigma = 1/(c_{s,\max}^+ L^+ \varepsilon_s^+ A)$, where θ_j denotes the j-th component of the parameter vector. Under these conditions, only the negative electrode state $x = x^-$ is required. The nomenclature for all the electrochemical model parameters is reported in the Appendix.

The state function is linear and it takes the form

$$f(\theta, x(k), u(k)) = A(\theta)x(k) + B(\theta)u(k), \tag{4}$$

where state matrices, are given by:

$$A(\theta) = \begin{bmatrix} 1 & 0 \\ T_s \theta_3 a_1 & 1 - T_s \theta_3 a_1 \end{bmatrix}, B(\theta) = \frac{T_s}{\theta_1} \begin{bmatrix} b_1 \\ b_2 \end{bmatrix}, \tag{5}$$

where T_s is the sampling time and with

$$a_1 = \frac{1}{\beta(1-\beta)}, \quad b_1 = \frac{1}{c_{s,\max}^-} \frac{1}{FL^-}, \quad b_2 = \frac{b_1}{1-\beta}.$$

The nonlinear output function takes the form

$$h(\theta, x(k), u(k)) = \eta_s^+(\theta, x(k), u(k)) - \eta_s^-(\theta, x(k), u(k)) \\ + U_s^+(\theta, x(k)) - U_s^-(\theta, x(k)) + (\theta_2/\theta_1)d_1 u(k), \tag{6}$$

where the nonlinear functions $\eta_s^\pm$ and $U_s^\pm$ are the surface overpotential and the open-circuit potential, respectively, with superscript $+$ for positive and $-$ for negative electrode, and $d_1 = R^-/(3L^-)$. Function $\eta_s^\pm$ is given by

$$\eta_s^\pm(\theta, u, x) = \frac{R_g T_{\text{ref}}}{\alpha_0 F} \sinh^{-1}\left(\frac{\mp R^\pm}{6\varepsilon_s^\pm L^\pm j_{n,0}^\pm(x_\pm)} u\right),$$

where the exchange current density is

$$j_{n,0}^\pm(x^\pm) = k_n^\pm c_{s,\max}^\pm \sqrt{c_e} \sqrt{x^\pm(\theta)\left(1 - x^\pm(\theta)\right)}.$$

Function $U_s^\pm$ is empirical and it depends on the considered electrode chemistry [1].

This EHM (1),(2) in healthy mode describes the ideal (desired) electrochemical reactions for a lithium-ion battery. However, batteries degrade over time due to undesired reactions and material fatigue, which is accounted for next.

B. Faulty operation

There are different sources of possible degradation that can take place during battery usage. Among the most important ones, we can refer to (i) capacity fade and (ii) power fade, which are the faults considered in this work. Notice that the battery cycle life can be very different from battery to battery, even if they come from the same manufacturing batch [26]. Early detection of small internal faults can help to separate the batteries with the best performance from the rest, which would narrow the battery cycle life variations.

Some electrochemical mechanisms that are responsible for these aging phenomena have been identified, while others are difficult to pinpoint. In the following, we introduce side reactions, as they are the most relevant and widely-known mechanism that degrades Li-ion batteries, and then we explain how we account for other, more uncertain, mechanisms.

1) Side reactions: In Li-ion batteries, not all the available lithium is effectively used to charge/discharge the battery but part of it is irreversibly consumed in side reactions. These reactions compete with the battery desired intercalation reactions, which can be modelled with Kirchhoff's law as

$$z(k) = u(k) + d(k) \tag{7}$$
$$0 = g(\theta, x(k), u(k), d(k)) \tag{8}$$

where $z(t)$ is the total current flowing through the battery terminals, and $u(t)$ and $d(t)$ are the internal main intercalation reaction and undesired side reaction currents, respectively. The nonlinear function in (8) takes the form

$$g(\theta, x(k), u(k), d(k)) = U_s^-(\theta, x(k))$$
$$+ \eta_s^-(\theta, x(k), u(k)) - U_{sr} - \eta_{sr}(d(k)), \qquad (9)$$

which represents the side reaction taking place at the negative electrode surface [27], [28], where U_{sr} is a constant that characterizes the occurrence of the side reaction and $\eta_{sr}(d(k))$ is given by

$$\eta_{sr}(d) = -\frac{R_g T_{\text{ref}}}{\alpha_0 F} \ln \left(-\frac{R^-}{3 L^- j_{sr,0}} d \right).$$

Under side reaction conditions, the nonlinear output function $h(\theta, x(k), u(k))$ in (6) is now given by

$$\overline{h}(\theta, x(k), u(k), z(k)) = \eta_s^+(\theta, x(k), z(k)) - \eta_s^-(\theta, x(k), u(k))$$
$$+ U_s^+(\theta, x(k)) - U_s^-(\theta, x(k)) + (\theta_2/\theta_1) d_1 z(k), \qquad (10)$$

which associates the total current $z(k)$ to the positive electrode and only the main intercalation reaction current $u(k)$ to the negative electrode. Notice that only the negative electrode suffers from the side reaction, since part of the total current $z(k)$ is lost through $d(k)$ while the positive electrode exploits all the current, i.e. $z(k)$ effectively reflects the main intercalation reaction in the positive electrode.

The amount of capacity lost due to the side reaction is

$$Q_{\text{loss}}(k+1) = Q_{\text{loss}}(k) - \frac{A}{3600} d(k),$$

which decreases the lithium inventory n_{Li} according to

$$n_{Li,t}(k) = n_{Li} - \frac{3600}{F} Q_{\text{loss}}(k)$$

affecting the cell balance of lithium (note that $n_{Li,t}(k)$ substitutes for $\theta_4 = n_{Li}$ when simulating the side reaction). The film resistance growth due to lithium consumption is ignored here.

2) Parameter variations: Besides side reactions, other degradation phenomena are likely to occur in Li-ion batteries, such as loss of active material, electrode morphological changes, electrolyte decomposition, and others [2], [28]. Even if some efforts have been devoted to identify these mechanisms and derive models to describe them, most of these models are empirical in nature [28], do not account for each source of degradation and do not fully characterize their complex intertwined behaviour. Therefore, instead of considering explicit models for other degradation sources such as in point 1) above, we evaluate the performance of the proposed FDI system through specific parametric changes affecting $\theta = [\varepsilon_s \ R_f \ g_s \ n_{Li}]^\top$. These parameter variations physically reflect common sources of battery deterioration, like loss of active material ε_s, impedance increase R_f, sluggish diffusion g_s and loss of lithium inventory n_{Li}.

III. SENSITIVITY ANALYSIS

In this section, we present a sensitivity analysis [29] in order to study the identifiability of the battery model. This study aims at evaluating the difficulty of estimating a given parameter from real data , i.e. it investigates how informative is the data through the sensitivity of measured signals with respect to parameters, as well as the linear correlations among parameters. On the one hand, if a model output is not sensitive to a given parameter change, then the parameter cannot be identified. On the other hand, if two sensitivity functions are linearly dependent, then the parameters are correlated and it is difficult to identify them individually.

Let us consider the discrete-time system (1),(2). The discrete-time sensitivity variables of the state $x \in \mathbb{R}^2$ and output $y \in \mathbb{R}$ with respect to the parameters $\theta \in \mathbb{R}^4$ are given by

$$s^x(k) = \frac{\partial x(k)}{\partial \theta} \in \mathbb{R}^{2 \times 4}, \quad s^y(k) = \frac{\partial y(k)}{\partial \theta} \in \mathbb{R}^{1 \times 4}. \quad (11)$$

These sensitivity variables evolve according to the sensitivity system associated with the model (1),(2), which takes the form

$$s^x(k+1) = \nabla_x f(\theta, x(k), u(k)) s^x(k) + \frac{\partial}{\partial \theta} f(\theta, x(k), u(k)), \quad (12)$$

$$s^y(k) = \nabla_x h(\theta, x(k), u(k)) s^x(k) + \frac{\partial}{\partial \theta} h(\theta, x(k), u(k)). \quad (13)$$

The sensitivities in (11) can be used to build the discrete-time sensitivity matrix [29] as

$$S^y = [s_1^y \ s_2^y \ \cdots \ s_{n_\theta}^y] \qquad (14)$$

where $s_j^y \in \mathbb{R}^N$ is the column vector formed by the sensitivity of the model output with respect to the j-th parameter for data of size N. Matrix S^y is analyzed thanks to the following decomposition $(S^y)^\top S^y = D^\top C D$ [30], where matrices C and D are given by

$$D = \text{diag} \left(\|s_1^y\|, \|s_2^y\|, \ldots, \|s_{n_\theta}^y\| \right), \qquad (15)$$

$$C = \begin{bmatrix} 1 & c_{12} & c_{13} & \cdots & & c_{1,n_\theta} \\ c_{21} & 1 & c_{23} & & & c_{2,n_\theta} \\ c_{31} & c_{32} & \ddots & & & \vdots \\ \vdots & & & 1 & & c_{n_\theta-1,n_\theta} \\ c_{n_\theta,1} & c_{n_\theta,2} & \cdots & c_{n_\theta,n_\theta-1} & & 1 \end{bmatrix}. \quad (16)$$

In matrix C, $c_{ji} = \dfrac{\langle s_j^y, s_i^y \rangle}{\|s_j^y\| \|s_i^y\|}$ for $j \neq i$ with $i = 1, \ldots, n_\theta$ for each $j = 1, \ldots, n_\theta$, $\| \cdot \|$ is the Euclidian norm and $\langle \cdot, \cdot \rangle$ is the inner product [30]. From this matrix decomposition we can infer linear dependencies among parameters. If $|c_{ji}|$ is close to 1, then parameters θ_j and θ_i are strongly linearly dependent. Conversely, values of c_{ji} close to zero imply orthogonality [12].

IV. OBSERVER-BASED RESIDUALS

We now proceed to design a state observer for the discrete-time EHM, which is then exploited for FDI, characterized by changes in degradation-related parameters. Consider a system similar to (1),(2) but as a stochastic system, i.e. including noise terms w and v in the state and output equations, respectively, such as in

$$x_s(k+1) = f(\theta, x_s(k), u(k)) + w(k) \qquad (17)$$

$$y_s(k) = h(\theta, x_s(k), u(k)) + v(k), \qquad (18)$$

where the noise sequences abide by $w(k) \sim \mathcal{N}(0, Q_x)$ and $v(k) \sim \mathcal{N}(0, R_x)$, with $\mathbb{E}[w(k)v(l)^\top] = 0$, where $\mathbb{E}(\cdot)$ is the expectation operator.

Due to the system nonlinearities, an unscented Kalman filter (UKF) is designed, which is reported in Table III in the Appendix. The UKF relies on the assumption that the distribution of the state vector and the observations are Gaussian. To present the algorithm, let us define the state as the concatenation of the original state and the process and measurement noise as

$$x_s^a(k) = [x_s(k)^\top \ w(k)^\top \ v(k)^\top]^\top \in \mathbb{R}^L,$$

where $L = 2n_x + n_y$ with n_x and n_y as the state and output dimensions, respectively. The state distribution is represented by a minimal set of carefully chosen sample points, called sigma points, which are denoted as

$$\mathcal{X}^a(k) = [\mathcal{X}(k)^\top \ \mathcal{X}^w(k)^\top \ \mathcal{X}^v(k)^\top]^\top.$$

These points are generated by a deterministic sampling procedure known as unscented transformation. The sigma point generation step is in (36), where $\hat{x}_s^a(k-1) \pm \gamma \sqrt{P_x^a(k-1)}$ stands for

$$\hat{x}_s^a(k-1) \pm \gamma \left(\sqrt{P_x^a(k-1)} \right)_l, l = 1, \ldots, L$$

where $(\cdot)_l$ is the l-th column of the matrix. The sigma points completely capture the true mean and covariance of the prior random variable. When the sigma points are propagated through the nonlinear system, a posterior mean and covariance that are accurate up to the second order are obtained.

The UKF is used to generate residuals for the FDI using the local approach. Under the assumption that

(A1) the parameter θ is locally identifiable at the nominal value $\theta = \theta_0$ [31],

we can define a residual related to θ as [31]

$$H(\theta, y_s(k), \hat{y}_s(k)) = s^y(k)^\top r(k), \qquad (19)$$

which minimizes the square of the output error. This residual is composed of two parts. The first one is the sensitivity of the model output y with respect to the parameter vector θ given by s^y in (11) but evaluated at $\hat{y}_s$. The output sensitivity $s^y(k)$ can be computed by resorting to the sensitivity system (12),(13), where the estimates of the state $\hat{x}_s$ coming from the UKF are substituted for $x(k)$. The second part is the innovation sequence defined as

$$r(k) = y_s(k) - \hat{y}_s(k). \qquad (20)$$

V. FDI DESIGN BASED ON LOCAL APPROACH

In this section, we consecutively develop a fault detection and fault isolation strategy based on the local approach [32] by exploiting the residual $H(\theta, y_s(k), \hat{y}_s(k))$ defined in (19).

Even in simple cases with linear models, the distribution of $H(\theta, y_s(k), \hat{y}_s(k))$ is often unknown. This issue can be bypassed by approximating this distribution asymptotically. One relevant approximation consists of assuming a small change in the parameter, which is known as the local approach [24]. Following this approach, for residual $H(\theta, y_s(k), \hat{y}_s(k))$ to be a valid primary residual for monitoring parameter vector θ, the following assumptions need to hold [32]:

(A2) it is a function differentiable in θ;

(A3) it satisfies the following conditions:

$$\mathbb{E}_\theta \ H(\theta, y_s(k), \hat{y}_s(k)) = 0 \quad \text{if} \quad \theta = \theta_0, \qquad (21)$$

$$\mathbb{E}_\theta \ H(\theta, y_s(k), \hat{y}_s(k)) \neq 0 \quad \text{if} \quad \theta \in v(\theta_0) \backslash \theta_0, \quad (22)$$

where $\mathbb{E}_\theta$ is the expectation when the system parameter value is θ and $v(\theta_0)$ is a neighborhood of the nominal parameter value θ_0.

This primary residual is then normalized as

$$\zeta_N(\theta) = \frac{1}{\sqrt{N}} \sum_{k=1}^{N} H(\theta, y_s(k), \hat{y}_s(k)). \qquad (23)$$

Assume further that [32]

(A4) the sensitivity matrix[2]

$$M(\theta_0) = \mathbb{E}_{\theta_0} \frac{\partial}{\partial \theta} H(\theta, y_s(k), \hat{y}_s(k)) \qquad (24)$$

exists and is full rank;

(A5) the limiting covariance matrix

$$\Sigma(\theta_0) = \lim_{N \to \infty} \mathbb{E}_{\theta_0} \zeta_N(\theta_0) \zeta_N^\top(\theta_0). \qquad (25)$$

exists and is positive definite.

Then, the normalized residual has remarkable asymptotic statistical properties as stated below.

A. Fault detection

To detect small changes in the system parameters θ, the local approach is used to discern between the following two local hypotheses:

$$\text{H}_0: \quad \theta = \theta_0, \qquad (26)$$

$$\text{H}_1: \quad \theta = \theta_0 + \frac{\eta}{\sqrt{N}}, \qquad (27)$$

where η is an unknown but constant vector and N is the sample size of the data.

The normalized residual $\zeta_N(\theta)$ defined in (23) can be proven to be asymptotically Gaussian distributed under both

---

[2]This sensitivity matrix M is for the primary residual-parameter relationship and should not be confused with the state-parameter sensitivity matrix S^y in (14).

hypotheses in (26),(27) [31], i.e. the following central limit theorem holds when $N \to \infty$ [24], [33],

$$\zeta_N(\theta_0) \to \begin{cases} \mathcal{N}(0, \Sigma(\theta_0)) & \text{under } H_0, \\ \mathcal{N}(-M(\theta_0)\eta, \Sigma(\theta_0)) & \text{under } H_1, \end{cases} \quad (28)$$

where the matrices $M(\theta_0)$ and $\Sigma(\theta_0)$ are defined in (24) and (25), respectively. Basically, the local approach performs a sensitivity analysis of the residual with respect to a fault, relative to the residual variance.

The asymptotic Gaussianity of the primary residual in (28) opens the door to design asymptotically optimum tests between composite hypothesis [24]. For instance, the decision between H_0 and H_1 in (26),(27) can be achieved through the optimum test statistics

$$\chi^2 = \zeta_N^\top \Sigma^{-1} M (M^\top \Sigma^{-1} M)^{-1} M^\top \Sigma^{-1} \zeta_N \quad (29)$$

with $\Sigma = \Sigma(\theta_0)$, $M = M(\theta_0)$ and $\zeta_N = \zeta_N(\theta_0)$, which is asymptotically χ^2-distributed as $N \to \infty$, with n_θ degrees of freedom. The limiting χ^2-distribution is central under H_0 and has a $\eta^\top M^\top \Sigma^{-1} M \eta$ non-centrality parameter under H_1.

B. Fault isolation

The isolation of a given fault is performed once the global χ^2-test has detected it. Let us assume that $\zeta_N \sim \mathcal{N}(M\eta, \Sigma)$ and the number n_a of elements of θ subject to change is known. Fault isolation is achieved by testing among the n_a-size subvector of η which one is non zero, c.f. if detection has taken place there should be one non zero situation. To this end, partition η as

$$\eta = \begin{bmatrix} \eta_a^\top & \eta_b^\top \end{bmatrix}^\top \quad (30)$$

with $\eta_a \in \mathbb{R}^{n_a}$ and $\eta_b \in \mathbb{R}^{n_b}$. Also assume that η_a is the sub-vector to be tested. Then we use the minmax test for fault isolation (FI), which consists in viewing the parameters in η_b as nuisances and statistically rejecting them. In this method, the nuisance parameters η_b are replaced by their least favorable value, i.e. the value that minimizes the power of the test, which is equivalent to the likelihood ratio [24]

$$\chi_a^{2*} = 2 \ln \frac{\max_{\eta_a, \eta_b} p_{\eta_a, \eta_b}(\zeta)}{\max_{\eta_b} p_{0, \eta_b}(\zeta)}. \quad (31)$$

Let

$$F = M^\top \Sigma^{-1} M$$

and partition it as

$$F = \begin{bmatrix} F_{aa} & F_{ab} \\ F_{ba} & F_{bb} \end{bmatrix} = \begin{bmatrix} M_a^\top \Sigma^{-1} M_a & M_a^\top \Sigma^{-1} M_b \\ M_b^\top \Sigma^{-1} M_a & M_b^\top \Sigma^{-1} M_b \end{bmatrix},$$

where $M = [M_a \ M_b]$ and M_a is made of the n_a columns associated to η_a. The residual of the linear regression of $\tilde{\zeta}_a = M_a^\top \Sigma^{-1} \zeta_N$ with respect to $\tilde{\zeta}_b = M_b^\top \Sigma^{-1} \zeta_N$ is

$$\zeta_a^* = \tilde{\zeta}_a - F_{ab} F_{bb}^{-1} \tilde{\zeta}_b.$$

Then, the minmax test in (31) can be shown to be

$$\chi_a^{2*} = \zeta_a^{*\top} F_a^{*-1} \zeta_a^* \quad (32)$$

where $F_a^* = F_{aa} - F_{ab} F_{bb}^{-1} F_{ba}$ is the covariance matrix of ζ_a^*. χ_a^{2*} is a χ^2-test with n_a degrees of freedom.

VI. SIMULATION RESULTS

In this section, we present the results obtained when considering a simulated Li-ion battery with graphite/LCO chemistry and whose model parameters are publicly available [34]. The sampling time was set to $T_s = 1$ s. The identifiability properties of the EHM are firstly discussed under a drive cycle (DC) discharge/charge scenario. Then, we present the fault detection (FD) and fault isolation (FI) results obtained when resorting to the asymptotic local approach.

A. Identifiability analysis

First, we verified the local structural identifiability of our nonlinear system (1),(2) (assumption A1) through differential geometry [35]. This check is not reported here due to lack of space. Next, we carried out a sensitivity analysis, whose results are shown in Fig. 1. The nonlinear EHM (1),(2) alongside the sensitivity system (12),(13) with sensitivities (11) were simulated under a drive cycle load. This load consisted of battery discharge/charge (Fig. 1a) using a UDDS (urban dynamometer driving schedule) profile, which was scaled (maximum current of $10C$, $1.8C$ average) to cover from 0.97 to 0.25 SOC of the battery during the first discharge. After the first drive cycle discharge, the current profile was inverted for charging and two consecutive charge/discharge cycles were performed. This was done to guarantee a long (more than 5×10^3 data samples, 80 min) persistent excitation. Figure 1b depicts the trajectories of the output relative sensitivity variables with respect to each considered parameter $\theta = [\varepsilon_s \ R_f \ g_s \ n_{Li}]^\top$. From the figure it follows that the sensitivity of R_f is clearly the largest one, followed by the one of g_s with the largest sensitivity levels during a few intervals. Then, ε_s sensitivity follows and n_{Li} is the least sensitive parameter (figure inset). This sensitivity ranking is confirmed by matrix $D = \text{diag}(134.054, 568.042, 343.068, 59.173)$ in (15).

Next, linear dependencies among parameters are assessed by computing the C matrix in (16), resulting in

$$C = \begin{bmatrix} 1.000 & -0.306 & 0.305 & -0.981 \\ -0.306 & 1.000 & -0.315 & 0.172 \\ 0.305 & -0.315 & 1.000 & -0.203 \\ -0.981 & 0.172 & -0.203 & 1.000 \end{bmatrix}, \quad (33)$$

The most correlated parameters are by far ε_s and n_{Li} with $c_{14} = -0.981$, followed by ε_s, R_f and g_s with $|c_{ji}| \approx 0.30$, $j \in \{1, 2\}$ and $i \in [2, 3]$ with $i \neq j$.

B. Fault detection and isolation

The FDI simulation is based on the EHM (1),(2) as plant model and the drive cycle as input current. Five faulty cases were considered, which are denoted as f_{θ_j} for a fault f affecting parameter θ_j (e.g. f_{ε_s} for $\theta_1 = \varepsilon_s$) with $j = 1, \ldots, 4$, while the fifth fault incorporates the side reaction in the model equations, i.e. side reaction current $d(k) \neq 0$, and it is denoted as $f_{d(k)}$. Note that the last fault is outside the formalism presented for the local approach, but it is intended to demonstrate how the algorithm performs when faced against more complex types of faults that might affect battery

	θ_0	f_{ε_s}	f_{R_f}	f_{g_s}	$f_{n_{Li}}$	$f_{d(k)}$	$f_{R_f}, 0.2\%$	$f_{g_s}, 5\%$	$f_{d(k)}{}^a$
					Fault detection				
χ^2	9.750	**39.660**	**20.113**	10.310	**14.761**	9.673	**44.680**	**16.220**	**24.972**
					Minmax test				
ε_s	3.434	3.456	4.041	3.624	**9.144**	3.198	3.087	**7.953**	**10.872**
R_f	3.040	**12.631**	5.494	2.862	**8.305**	2.617	**16.869**	5.901	**19.768**
g_s	2.738	5.429	2.997	2.128	2.011	2.499	3.797	**8.979**	2.922
n_{Li}	3.297	3.375	3.937	3.453	**8.831**	3.097	2.945	**8.017**	10.574

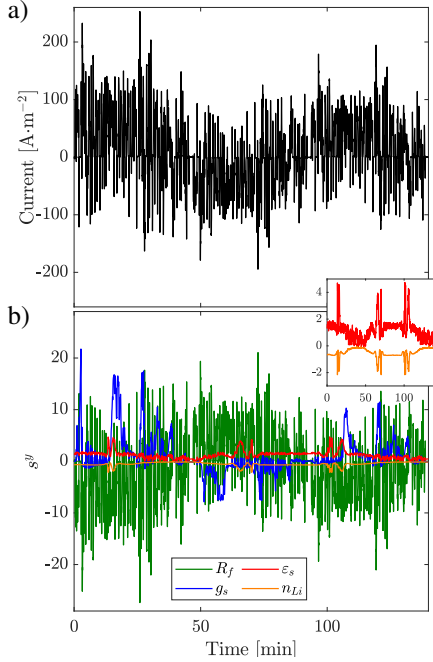$^a j_{sr,0} = 3 \times 10^{-5}$ A·m^{-2}.

a)

b)

Fig. 1. Relative sensitivity analysis of the EHM with respect to the considered parameter vector for a drive cycle battery discharge/charge. a) Input current profile and b) trajectories of the output sensitivity variables with respect to each parameter.

operation. Unless otherwise stated, the model parameters were varied by $\Delta\theta = 0.1\%$ relative error with respect to their nominal values θ_0 whereas the side reaction exchange current density $j_{sr,0} = 1.5 \times 10^{-6}$ A·m^{-2} [27]. These parameters translate into a maximum capacity fade of 0.07% and ohmic drop of 0.004% when a fully charged battery is discharged in simulation at $C/2$. The voltage signal was corrupted with a white noise sequence of variance $R = 10$ mV^2 in all cases.

The UKF tuning parameters were selected to be $\alpha = 0.1$, $\beta = 2$ and $\kappa = 3 - L$ [36]. The state vector was initialized with -5% error. The measurement noise variance was set to its actual value, whereas the process noise variance was set to $Q = 10^{-8}I_2$ and the initial error covariance matrix was $P_{x,0} = 10^{-3}I_2$, which provided good convergence of the filter in simulation.

For each simulation of the FDI system, the sample size was $N = 8400$ from which we discarded the first 200 samples to avoid transient effects. The implementation of the algorithm is done in batch, i.e. a given time series of data is processed at a time, and it could be performed periodically for FDI. For each considered parameter value, either nominal

or changed, 100 simulations were carried out with different measurement noise realizations. The estimation of matrix $\Sigma(\theta_0)$ in (25) from available data is not a trivial problem as pointed out in [31], [24]. We computed it here as [31]

$$\Sigma \approx \frac{1}{N}\sum_{k=1}^{N} H_k H_k^\top + \sum_{i=1}^{n_i} \frac{1}{N-i}\sum_{k=1}^{N-i}\left(H_k H_{k+i}^\top + H_{k+i}H_k^\top\right).$$
(34)

We set $n_i = 12$, which ensures that Σ is positive definite. Matrix M in (24) is estimated by [31]

$$M \approx \frac{1}{N}\sum_{k=1}^{N}\left[-s^y(k)^\top s^y(k) + r(k)s^{yy}(k)\right]_{\theta=\theta_0}.$$
(35)

where s^{yy} denotes second-order sensitivities of the model output y with respect to the parameter vector θ. The sensitivity equations were computed with CasADI [37], which is automatic differentiation software able to calculate first and second-order derivatives efficiently.

Table I shows the FD results for the χ^2-test and the FI results for the minmax test under nominal (first column entry) and slightly changed ($\Delta\theta = 0.1\%$ in second to sixth column entries) parameter values. That level of parameter variation translates into overall faults of f $= [-600\ 10\ -3\ -2000] \times 10^{-6}$ where f $= [f_{\varepsilon_s}\ f_{R_f}\ f_{g_s}\ f_{n_{Li}}]$. From these results it follows that it is possible to detect faults affecting ε_s, R_f and n_{Li}. The largest χ^2 value is obtained for ε_s instead of the most sensitive parameter R_f, which is due to the 60 times larger fault in absolute value for the former parameter. Similarly, despite the large and small sensitivities of g_s and n_{Li}, respectively, their faults are the smallest and biggest ones which prevents and helps their respective detection. No parameter can be correctly isolated, with ε_s fault ascribed to R_f. Moreover, n_{Li} is associated with changes in n_{Li} itself, ε_s and R_f, which can be explained by the low sensitivity of n_{Li} and its high correlation with ε_s, while the influence of R_f seems to be limited given the lower value of its indicator w.r.t. n_{Li} and ε_s. In order to test if larger fault magnitudes can be picked up by the algorithm for the remaining undetected and non-isolated faults, we increase $\Delta\theta = 0.2\%$ for R_f, $\Delta\theta = 5\%$ for g_s and $j_{sr,0} = 3 \times 10^{-5}$ A·m^{-2} for the side reaction. The results are shown in the last three columns of Table I. Under these changes, now the χ^2-test is able to detect these faults. While the isolation of R_f is now correct, the indicator of g_s becomes activated for ε_s, n_{Li} and g_s itself with the latter having a slight edge over
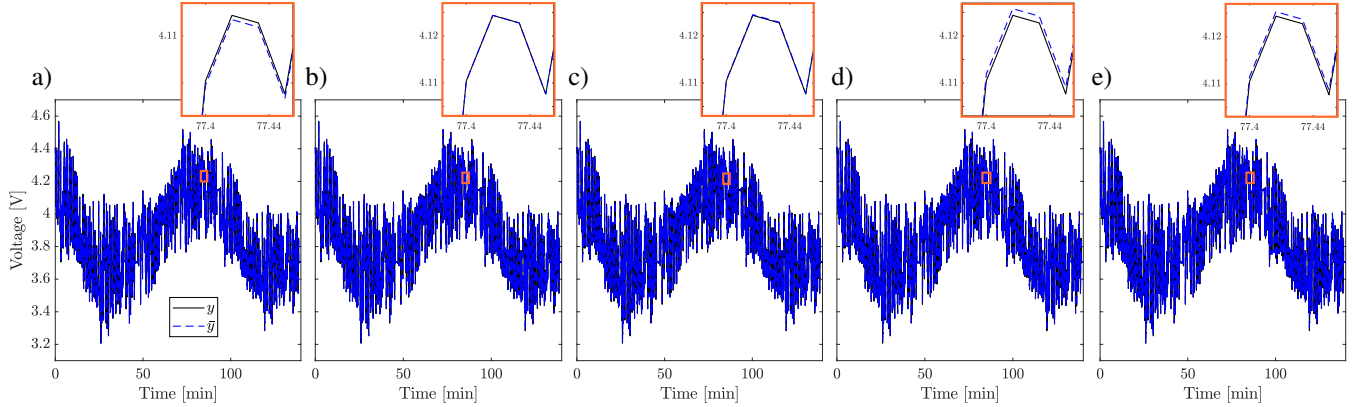
Fig. 2. Voltage output responses under drive cycle. Both healthy y and faulty $\bar{y}$ modes are shown. Different faulty behaviours are depicted, namely parameter variations of a) $\Delta\theta = 0.1\%$ in ε_s and b) R_f, c) $\Delta\theta = 5\%$ in g_s, d) $\Delta\theta = 0.1\%$ in n_{Li} and e) side reaction of $j_{sr,0} = 3 \times 10^{-5}$ A·m^{-2}.

the former ones. Finally, the side reaction is ascribed mainly to R_f. Since the side reaction can be seen as a perturbation to the input current and R_f appears as input coefficient in the model, this allocation is logical.

To give an idea of how small the considered fault magnitudes are, and how difficult is to detect/isolate them, Fig. 2a-e shows the model output when the system is healthy (solid black curves) and when it is subject to a given fault (dashed blue curves). The five faulty scenarios are depicted. The worst fault cases in Table I are considered for each parameter. The figure shows that the different faults are imperceptible from the voltage standpoint for the naked eye (overlapping curves), with a capacity fade and an ohmic drop of up to 0.15% and 0.004%, respectively. Only when a considerable zoom is applied (figure insets) it is possible to see slight changes in the voltage trajectories from healthy to faulty modes.

VII. CONCLUSIONS

A diagnosis scheme aiming at detecting and isolating small faults characterizing lithium-ion battery degradation has been reported. This scheme relies on the asymptotic local approach. First, a reduced-order electrochemical model of the battery under both healthy and faulty conditions was used, and its identifiability properties were verified. Secondly, a state observer was used to generate primary residuals along with the limiting covariance matrix. Finally, the residuals were exploited by χ^2-tests for FDI. It was verified that the sensitivity of the parameters is large with an aggressive drive cycle. All the considered parameter changes can be successfully detected, even if some relative faults need to be larger than 0.1% to do so. The most sensitive parameters are the volume fraction and moles of lithium, which facilitates the FDI of these faults. On the other hand, the isolation of less sensitive and highly correlated parameters might be erroneous. Overall, detection of small degradation rates causing less than 0.15% capacity fade and 0.004% resistance increase can be achieved, which is well below the accuracy of experimental procedures to measure capacity/resistance. The proposed method might also be particularly useful for the early warning of small battery internal faults that may

condition the entire cycle life of a battery, which we will pursue in future work.

APPENDIX

The nomenclature and UKF algorithm are now reported.

TABLE II

NOMENCLATURE.

Parameter	Symbol
Cross-sectional area [m^2]	A
Maximum lithium concentrations [mol.m^{-3}]	$c_{s,\max}^{\pm}$
Electrolyte concentrations [mol.m^{-3}]	c_e
Faraday's constant [C·mol^{-1}]	F
Diffusion time constant inverse [s^{-1}]	g_s
Side reaction exchange current density [A.m^{-2}]	$j_{sr,0}$
Reaction rate constant [A.m$^{2.5}$.mol$^{-1.5}$]	$k_n^{\pm}$
Electrode thickness [m^2]	$L^{\pm}$
Particle Radius [m]	$R^{\pm}$
Film resistance [Ω.m^2]	R_f
Universal gas constant [J·mol^{-1}·K^{-1}]	R_g
Reference temperature [K]	T_{ref}
Apparent transfer coefficient [-]	α_0
Particle volume ratio [-]	β
Active material volume fraction [-]	ε_s

REFERENCES

[1] N. A. Chaturvedi, R. Klein, J. Christensen, J. Ahmed, and A. Kojic. Algorithms for advanced battery-management systems. *IEEE Control Systems*, 30(3):49–68, 2010.

[2] X. Hu, K. Zhang, K. Liu, X. Lin, S. Dey, and S. Onori. Advanced fault diagnosis for lithium-ion battery systems (v1). *TechRxiv*, 2020.

[3] S. Santhanagopalan, Q. Zhang, K. Kumaresan, and R.E. White. Parameter estimation and life modeling of lithium-ion cells. *Journal of The Electrochemical Society*, 155(4):A345–A353, 2008.

[4] V. Ramadesigan, K. Chen, N. A. Burns, V. Boovaragavan, R. D. Braatz, and V. R. Subramanian. Parameter estimation and capacity fade analysis of lithium-ion batteries using reformulated models. *Journal of The Electrochemical Society*, 158(9):A1048–A1054, 2011.

[5] F. Sun and R. Xiong. A novel dual-scale cell state-of-charge estimation approach for series-connected battery pack used in electric vehicles. *Journal of Power Sources*, 274:582–594, 2015.

[6] C. Zhang, W. Allafi, Q. Dinh, P. Ascencio, and J. Marco. Online estimation of battery equivalent circuit model parameters and state of charge using decoupled least squares technique. *Energy*, 142:678–688, 2018.

[7] W. Allafi, K. U.ddin, C. Zhang, R. Mazuir Raja Ahsan Sha, and J. Marco. On-line scheme for parameter estimation of nonlinear lithium ion battery equivalent circuit models using the simplified refined instrumental variable method for a modified wiener continuous-time model. *Applied Energy*, 204:497–508, 2017.

TABLE III

UKF FOR THE NONLINEAR MODEL IN (17),(18)†.

Initialization: for $k = 0$, set

$\hat{x}_{s,0} = E[x_{s,0}], \quad P_{x,0} = E[(x_{s,0} - \hat{x}_{s,0})(x_{s,0} - \hat{x}_{s,0})^\top]$

$\hat{x}_{s,0}^a = E[x_{s,0}^a] = [\hat{x}_{s,0}^\top \quad 0 \quad 0]^\top$

$P_{x,0}^a = E[(x_{s,0}^a - \hat{x}_{s,0}^a)(x_{s,0}^a - \hat{x}_{s,0}^a)^\top] = \mathrm{diag}(P_{x,0}, Q_x, R_x)$

Computation: for $k = 1, 2, \ldots$ compute

Sigma points:

$$\mathcal{X}_{k-1}^a = \begin{bmatrix} \hat{x}_{s,k-1}^a & \hat{x}_{s,k-1}^a + \gamma\sqrt{P_{x,k-1}^a} & \hat{x}_{s,k-1}^a - \gamma\sqrt{P_{x,k-1}^a} \end{bmatrix} \quad (36)$$

Time-update:

$$\mathcal{X}_{k|k-1} = f(\theta, \mathcal{X}_{k-1}, u_k) + \mathcal{X}_{k-1}^w \quad (37)$$

$$\hat{x}_{s,k}^- = \sum_{l=0}^{2L} W_l^{(m)} \mathcal{X}_{l,k|k-1} \quad (38)$$

$$P_{x,k}^- = \sum_{l=0}^{2L} W_l^{(c)} \left(\mathcal{X}_{l,k|k-1} - \hat{x}_{s,k}^-\right)\left(\mathcal{X}_{l,k|k-1} - \hat{x}_{s,k}^-\right)^\top \quad (39)$$

Measurement-update

$$\mathcal{Y}_{k|k-1} = h(\theta, \mathcal{X}_{k|k-1}, u_k) + \mathcal{X}_{k-1}^v \quad (40)$$

$$\hat{y}_{s,k} = \sum_{l=0}^{2L} W_l^{(m)} \mathcal{Y}_{l,k|k-1} \quad (41)$$

$$P_{y,k} = \sum_{l=0}^{2L} W_l^{(c)} \left(\mathcal{Y}_{l,k|k-1} - \hat{y}_{s,k}\right)\left(\mathcal{Y}_{l,k|k-1} - \hat{y}_{s,k}\right)^\top \quad (42)$$

$$P_{xy,k} = \sum_{l=0}^{2L} W_l^{(c)} \left(\mathcal{X}_{l,k|k-1}^x - \hat{x}_{s,k}^-\right)\left(\mathcal{Y}_{l,k|k-1} - \hat{y}_{s,k}\right)^\top \quad (43)$$

$$\mathcal{K}_k = P_{xy,k} P_{y,k}^{-1}, \quad (44)$$

$$\hat{x}_{s,k} = \hat{x}_{s,k}^- + \mathcal{K}_k \left(y_{s,k} - \hat{y}_{s,k}\right), \quad (45)$$

$$P_{x,k} = P_{x,k}^- - \mathcal{K}_k P_{y,k} \mathcal{K}_k^\top, \quad (46)$$

Tuning parameters:

$$\gamma = \sqrt{L + \lambda}, \quad \lambda = \alpha^2(L + \kappa) - L,$$
$$W_0^{(m)} = \frac{\lambda}{L+\lambda}, \quad W_0^{(c)} = \frac{\lambda}{L+\lambda} + 1 - \alpha^2 + \beta,$$
$$W_l^{(m)} = W_l^{(c)} = \frac{1}{2(L+\lambda)}, \quad l = 1, \ldots, 2L, L = 2n_x + n_y \quad (47)$$

---

†For convenience, the discrete time argument k is written as a subscript in the table.

[8] G.L. Plett. Extended kalman filtering for battery management systems of LiPB-based HEV battery packs: Part 3. State and parameter estimation. *Journal of Power Sources*, 134(2):277–292, 2004.

[9] Y. Wang, H. Fang, L. Zhou, and T. Wada. Revisiting the state-of-charge estimation for lithium-ion batteries: A methodical investigation of the extended Kalman filter approach. *IEEE Control Systems*, 37(4):73–96, 2017.

[10] R. Restaino and W. Zamboni. Comparing particle filter and extended Kalman filter for battery state-of-charge estimation. In *IECON 2012 - 38th Annual Conference on IEEE Industrial Electronics Society*, pages 4018–4023, 2012.

[11] Y. Wang, H. Fang, Z. Sahinoglu, T. Wada, and S. Hara. Adaptive estimation of the state of charge for lithium-ion batteries: Nonlinear geometric observer approach. *IEEE Transactions on Control Systems Technology*, 23(3):948–962, 2015.

[12] S. J. Moura, N. A. Chaturvedi, and M. Krstić. Adaptive partial differential equation observer for battery state-of-charge/state-of-health estimation via an electrochemical model. *Journal of Dynamic Systems, Measurement, and Control*, 136(1):011015–1–011015–11, 2014.

[13] D. Zhang, S. Dey, H. E. Perez, and S. J. Moura. Remaining useful life estimation of lithium-ion batteries based on thermal dynamics. In *2017 American Control Conference*, pages 4042–4047, Seattle, WA, USA, 2017.

[14] L.D. Couto, J. Schorsch, N. Job, A. Léonard, and M. Kinnaert. State of health estimation for lithium ion batteries based on an equivalent-hydraulic model: An iron phosphate application. *Journal of Energy Storage*, 21:259–271, 2019.

[15] L. Zheng, L. Zhang, J. Zhu, G. Wang, and J. Jiang. Co-estimation of

state-of-charge, capacity and resistance for lithium-ion batteries based on a high-fidelity electrochemical model. *Applied Energy*, 180:424–434, 2016.

[16] W. Chen, W.-T. Chen, M. Saif, M.-F. Li, and H. Wu. Simultaneous fault isolation and estimation of lithium-ion batteries via synthesized design of Luenberger and learning observers. *Control Systems Technology, IEEE Transactions on*, 22(1):290–298, 2014.

[17] A. Sidhu, A. Izadian, and S. Anwar. Adaptive nonlinear model-based fault diagnosis of li-ion batteries. *IEEE Transactions on Industrial Electronics*, 62(2):1002–1011, 2015.

[18] Z. Liu and H. He. Sensor fault detection and isolation for a lithium-ion battery pack in electric vehicles using adaptive extended Kalman filter. *Applied Energy*, 185:2033–2044, 2017.

[19] S. Zhao, S. R. Duncan, and D. A. Howey. Observability analysis and state estimation of lithium-ion batteries in the presence of sensor biases. *IEEE Transactions on Control Systems Technology*, 25(1):326–333, 2017.

[20] S. Dey, S. Mohon, P. Pisu, and B. Ayalew. Sensor fault detection, isolation, and estimation in lithium-ion batteries. *IEEE Transactions on Control Systems Technology*, 24(6):2141–2149, 2016.

[21] G. Ablay. Online condition monitoring of battery systems with a nonlinear estimator. *IEEE Transactions on Energy Conversion*, 29(1):232–239, 2014.

[22] L.D. Couto and M. Kinnaert. Internal and sensor fault detection and isolation for Li-ion batteries. In *IFAC-PapersOnLine*, volume 51, pages 1431–1438, Warsaw, Poland, 2018.

[23] Z. Liu, Q. Ahmed, J. Zhang, G. Rizzoni, and H. He. Structural analysis based sensors fault detection and isolation of cylindrical lithium-ion batteries in automotive applications. *Control Engineering Practice*, 52:46–58, 2016.

[24] M. Basseville. Model-based statistical signal processing and decision theoretic approaches to monitoring. *IFAC Proceedings Volumes*, 36(5):1–12, 2003.

[25] M. Basseville and I. Nikiforov. *Detection of Abrupt Changes: Theory and Applications*. Information and System Sciences Series. Prentice-Hall, Englewood Cliffs, NJ, 1993.

[26] T. Baumhöfer, M. Brühl, S. Rothgang, and D.U. Sauer. Production caused variation in capacity aging trend and correlation to initial cell performance. *Journal of Power Sources*, 247:332–338, 2014.

[27] P. Ramadass, B. Haran, P.M. Gomadam, R. White, and B.N. Popov. Development of first principles capacity fade model for Li-ion cells. *Journal of the Electrochemical Society*, 151(2):A196–A203, 2004.

[28] J.M. Reniers, G. Mulder, and D.A. Howey. Review and performance comparison of mechanical-chemical degradation models for lithium-ion batteries. *Journal of The Electrochemical Society*, 166(14):A3189–A3200, 2019.

[29] A. Villaverde and A. Barreiro. Identifiability of large nonlinear biochemical networks. *MATCH Communications in Mathematical and in Computer Chemistry*, 76:259–296, 2016.

[30] B.F. Lund and B.A. Foss. Parameter ranking by orthogonalization—Applied to nonlinear mechanistic models. *Automatica*, 44(1):278–281, 2008.

[31] Q. Zhang, M. Basseville, and A. Benveniste. Fault detection and isolation in nonlinear dynamic systems: A combined input–output and local approach. *Automatica*, 34(11):1359–1373, 1998.

[32] Q. Zhang and M. Basseville. Monitoring nonlinear dynamical systems: A combined observer-based and local approach. In *Proceedings of the 37th IEEE Conference on Decision and Control*, volume 1, pages 1149–1154, 1998.

[33] A. Benveniste, M. Metivier, and P. Priouret. *Adaptive Algorithms and Stochastic Approximations*, volume 22 of *Stochastic Modelling and Applied Probability*. Springer-Verlag Berlin Heidelberg, 1990.

[34] J. Newman. Fortran programs for simulation of electrochemical systems., 2008.

[35] A.F. Villaverde, T. Nikolaos, and J.R. Banga. Full observability and estimation of unknown inputs, states and parameters of nonlinear biological models. *J. R. Soc. Interface*, 16, 2019.

[36] Eric A. Wan and Rudolph van der Merwe. *The Unscented Kalman Filter*, pages 221–280. John Wiley & Sons, Inc., 2002.

[37] J.A.E. Andersson, J. Gillis, G. Horn, J.B. Rawlings, and M. Diehl. CasADi: A software framework for nonlinear optimization and optimal control. *Mathematical Programming Computation*, 11(1):1–36, 2019.